Shot Noise

$\dot{N}$ = average rate

i^2 = Fluctuation^2 /Hz

$i^2 = 2\langle\dot{N}\rangle$

TABLE OF CONTENTS

MASSACHUSETTS INSTITUTE OF TECHNOLOGY
RESEARCH LABORATORY OF ELECTRONICS
CAMBRIDGE, MASS. 02139

August 8, 1974

Proposal to
National Science Foundation

"Interferometric Broad Band Gravitational Antenna"

Abstract

This proposal is for an NSF grant to continue the development of a broadband gravitational radiation antenna that uses free masses as antenna elements. The masses are the mirror mounts of a laser illuminated Michelson interferometer which is used to measure the gravitationally induced strains in space. Although the proposed scheme is in some regards technically more difficult than resonant bar antennas, it holds the promise of extending the search for gravitational radiation to a sensitivity such that one may expect to detect the radiation from various astronomical sources. The first step is a small prototype interferometric antenna with 9 meter arms. This prototype is at least 1000 times more sensitive to a large class of astronomical sources of gravitational radiation than existing resonant bar antennas; however, any reasonable estimates of the source strengths of known and imagined sources still indicate that the prototype antenna will only be able to set upper limits on the gravitational radiation intensity. It is hoped that the techniques developed can be used in interferometric antennas with baselines of the order of a kilometer or more, since the sensitivity of this type of antenna increases with the square of the baseline.

Preliminary work has been going on at M.I.T. for several years with the support of the Joint Services Electronics Program and the M.I.T. Sloan Fund. The JSEP has terminated support for the project as of June 1974 as it cannot justify the relevance of gravitational research to its own program. The proposal to the NSF is for operations costs for two years, the installation of the antenna at an off campus site and for data acquisition equipment.

Introduction

It is probably safe to say that gravitational radiation has not been detected to date. This is unfortunate, for had the Weber experiments[1,2,3,4] been confirmed by others[5,6,7,8,9,10], gravitational wave astronomy would have opened up a new window into the universe as well as provided a handle to test relativistic theories of gravitation.

Facing cold realities after the considerable theoretical work engendered by the Weber experiments, it now seems that a legitimate search for gravitational radiation from astronomical sources will require a substantial improvement in detector sensitivity, possibly by a factor of 10^4 to 10^6. A compilation of gravitational radiation sources and their hypothesized spectra is given in appendix 1.

At present there appear to be three approaches that may lead to gravitational wave astronomy with higher sensitivity, none of which is without problems. The first is the development of cooled, high Q bars. The assumption is that since the dominant noise in room temperature antennas is thermal noise, the overall system noise will scale with temperature. Even if this is true, cooled bars will require significant advances in

transducer technology to reach their ultimate potential. The second approach, complementary to the others, is to use many cross-correlated antennas, a scheme that gains sensitivity with the square root of the number of antennas. Thirdly and finally, is to use antennas employing large baselines to capitalize on the property that a gravitational wave creates a strain in space while the noise, is to first order independent of the baseline. For a given displacement noise, the minimum detectable gravitational wave intensity decreases with the square of the antenna baseline which is ultimately limited by the condition that the dimensions of the antenna must be less than or equal to the wavelength of the gravitational wave.

The basis of this proposal is the development of a small, interferometric antenna with 9 meter arms. Although the antenna is 1000 times more sensitive than existing gravitational wave detectors, it is viewed as a prototype of a much larger system with a baseline of a kilometer or more. The interferometric antenna is broad-band and therefore useful in detecting periodic, impulsive and broad-band gravitational radiation sources.

Theory of a Gravitational Wave Interacting with Free Masses

In his 1918 paper on gravitational waves Einstein[11] showed by a perturbation argument that a weak gravitational plane wave has an irreducible metric tensor in an almost Euclidean space. The total metric tensor is

$$g_{ij} = \eta_{ij} + h_{ij} \qquad (1)$$

where

$$\eta_{ij} = \begin{bmatrix} 1 & & & 0 \\ & -1 & & \\ & & -1 & \\ 0 & & & -1 \end{bmatrix} \qquad (2)$$

is the Minkowski background metric tensor. h_{ij} is the perturbation metric tensor due to the gravitational wave and it is assumed that all components of this tensor are much smaller than 1. If the plane wave propagates along the x_1 direction, it is always possible to find a coordinate system in which h_{ij} takes the irreducible form

$$h_{ij} = \left(\begin{array}{c|cc} 0 & 0 & \\ \hline 0 & h_{22} & h_{23} \\ & h_{32} & h_{33} \end{array}\right) \qquad (3)$$

with $h_{22} = - h_{33}$ and $h_{23} = h_{32}$. The tensor components have the usual functional dependence $f(x_1 - ct)$.

To gain some insight into the meaning of a plane gravitational wave, assume that the wave is in the single polarization state $h_{23} = h_{32} = 0$ and furthermore let $h_{22} = - h_{33} = h \sin (kx_1 - \omega t)$. The interval between two neighboring events is then given by

$$ds^2 = g_{ij}dx^i dx^j = c^2dt^2 - [dx_1^2 + (1 + h \sin(kx_1 - \omega t))dx_2^2 + (1 - h \sin(kx_1 - \omega t))dx_3^2] \qquad (4)$$

The metric relates coordinate distances to proper lengths. In this metric coordinate time is proper time; however, the spatial coordinates are not proper lengths. One can give some reality to the coordinates by placing free noninteracting masses at various points in space which then label the coordinates. The

proper distance between two coordinate points may then be defined by the light travel time between the masses. Let there be a light source at $x_2 = -\ell/2$ and a receiver at $x_2 = \ell/2$. For light the total interval is always zero so that

$$ds^2 = 0 = c^2dt^2 - (1 + h \sin(kx_1 - \omega t))dx_2^2 \qquad (5)$$

since $h << 1$

$$cdt = [1 + \frac{h}{2} \sin(kx_1 - \omega t)]dx_2 \qquad (6)$$

If the light travel time, Δt, is much less than the period of the wave, the integral for Δt becomes simple and one gets

$$\Delta t = (1 - \frac{h}{2} \sin \omega t)\frac{\ell}{c} \qquad (7)$$

In the absence of the gravitational wave $\Delta t = \ell_o/c = \ell/c$, the coordinate distance becomes the proper length. The variation in Δt due to the gravitational wave is given by

$$\delta\Delta t = (\frac{h}{2} \sin \omega t)\frac{\ell}{c} \qquad (8)$$

This can be interpreted as though the gravitational wave produces a strain in space in the x_2 direction of

$$\frac{\Delta\ell}{\ell_o} = \frac{h}{2} \sin \omega t = \frac{h_{22}}{2} \qquad (9)$$

There is a comparable strain in the x_3 direction, however inverted in phase.

The intensity of the gravitational wave in terms of the plane wave metric tensor is given by Landau and Lifshitz[12] as

$$I_g = \frac{c^3}{16\pi G}\left[\left(\frac{dh_{23}}{dt}\right)^2 + \frac{1}{4}\left(\frac{dh_{22}}{dt} - \frac{dh_{33}}{dt}\right)^2\right] \qquad (10)$$

For subsequent calculations, it is more useful to relate the power spectrum of the gravitationally induced displacement to the incident gravitational intensity spectrum.

$$x_g^2(\omega) = \frac{h^2(\omega)\,\ell_o^2}{4} = \frac{8\pi G \ell_o^2}{c^3 \omega^2} I_g(\omega) \qquad \ell_o < \lambda_g \qquad (11)$$

where l_o is the separation of the masses.

The Antenna Design

The principle idea of the antenna is to measure the geodesic deviation of free masses by passing light signals between them. The notion is not new; it has appeared as a Gedanken experiment in F.A.E. Pirani's[13] studies of the measurable properties of the Riemann tensor. However, it became a practical idea only with the advent of lasers and the realization that interferometric distance measurements could be made to a much higher precision than the wavelength of light. The limit is determined by the quantum limited shot noise (Poisson noise) arising from the granularity of light and the statistics of the detection process. It was quickly realized that interferometric gravitational wave antennas had several unique properties; they are broad-band detectors, can be extended to the optimal size of the gravitational wavelength and are not loaded by the displacement detectors.

Initial work on such antennas began at M.I.T. in 1970 as part of several senior thesis projects following the development of an experiment in 1967 that demonstrated shot noise limited interrogation of fringes in a laser illuminated Michelson interferometer[14].

For the last two years, the design and construction of the prototype antenna has been the Doctor's thesis of Mr. D. K. Owens at M.I.T. who has contributed substantive ideas to the project.

Work began at Hughes Aircraft under the direction of Dr. R. Forward on an interferometric antenna design for use in space at the instigation of Dr. Philip Chapman then of N.A.S.A. Houston and a frequent visitor to M.I.T. in early 1970. The work at Hughes culminated in a premature publication which did not do the idea justice but nevertheless demonstrated again that laser interferometers operating at the Poisson limit were feasible.[15]

A schematic drawing of the antenna being constructed at M.I.T. is shown in figure 1. Three masses are suspended on horizontal seismometer mounts in high vacuum ($P < 10^{-7}$ torr). The three masses are the mirror mounts of an equal arm Michelson interferometer illuminated by a commercial 1 watt Argon ion laser. Each interferometer arm is a 9 meter long reentrant optical delay line comprised of dielectric coated spherical mirrors in a near confocal configuration. The laser beam is split by a 50 - 50 beam splitter and enters the delay lines through a hole in the spherical mirrors. The beam makes approximately 300 passes in each cavity before reemerging through the same hole by which it entered. The emerging beam passes through Pockel's cell phase shifters and is recombined by the beam splitter after which it is detected by a water cooled PIN Silicon photo diode.

The interferometer is held on a fixed point of a fringe by a servo system using the Pockel's cell phase shifters as controllers. The servo error signal is derived by modulating the optical

phase in oppositely polarized Pockel's cells in the two interferometer arms by $\pm\pi/4$ at a 10MHz rate. The fringe phase modulation is synchronously demodulated yielding an error signal which is applied to the Pockel's cells to maintain the fringe modulation symmetry. The error signal is proportional to the differential displacement of the end masses and is the output of the antenna. With the servo operated in this manner as a nulling device the laser amplitude noise at frequencies other than the modulation frequency is suppressed, provided the open loop gain is high enough.

The dynamic range of the Pockel's cells is limited to phase shifts equivalent to a few wavelengths motion of the end masses. Two approaches can be taken to increase the dynamic range of the interferometer to accomodate long term drifts due to ground noise and temperature changes. The first is to employ a slow, large dynamic range controller to move the end masses, for example an electrostatic force applied to the end masses, to hold the interferometer on a single fringe. The second approach, which we have adopted for the small antenna, is to let the interferometer jump from one fringe to an equivalent point on the neighboring fringe when the error signal has reached a predetermined value. The fringe jumps are counted in an up-down counter, converted into analog signals and passed through a high pass filter. The low frequency cut off of this filter determines the low frequency response of the antenna. The output of this filter is added to the continuous fringe output signal and recorded as the antenna output. The fringe jumps take place in a time determined by the time constant of the Pockel's cell which is of the order of 10^{-8} seconds, during this time the post mixer analog circuitry is reset as well. By properly setting the timing and the error signal amplitude at which the fringe jump occurs, it is possible to make the transients in the antenna output comparable to the Poisson noise.

We have measured the amplitude noise of a Spectra Physics model 165 Argon Ion laser at various power levels with the laser oscillating in both multi and single longitudinal modes. Figure 2 shows the results of these measurements with the laser oscillating in a single longitudinal mode. At frequencies below 300KHz, the power spectrum of the amplitude noise is dominated by ion acoustic and plasma oscillations as well as spectral peaks at multiples of the power line frequency due to inadequate filtering in the power supply. At frequencies above 3MHz, the amplitude noise closely approaches the Poisson limit even at 1/2 watt output. The measurements were limited to a maximum of 1/2 watt because of the onset of space charge limited flow in the Silicon photodiode at higher power.

The frequency stability of the laser is not critical provided that the difference in optical delay in the two interferometer arms is less than the reciprocal of the oscillating laser line width. Typically, for the Argon laser a delay difference of 10^{-9} seconds (30cm) will contribute a displacement noise due to frequency instability that is less than 1/10 of the Poisson amplitude noise.

The multipass delay lines that comprise the interferometer arms are useful components in an interferometric antenna as long as the Poisson amplitude noise dominates the antenna noise budget and the delay line storage times remain less than 1/2 the period of the gravitational wave. For fixed laser power, the multi-pass arms increase the fringe phase sensitivity of the interferometer by the number of passes per arm. The number of passes is limited by the reflectivity and optical quality of the mirror surfaces.

As long as the Poisson amplitude noise is dominant, the optical delay line is equivalent to increasing the length of the antenna, however at those frequencies where noise sources,

such as thermal and ground noise, that physically move the end mass dominate, the only way to increase the signal-to-noise ratio is to actually increase the antenna baseline.

Optical delay lines using spherical mirrors have been described by Herriott[16]. D. K. Owens at M.I.T. has studied and constructed delay lines using spherical mirrors, a brief description of his results are given in appendix 2. He has discovered several interesting and useful properties of these delay lines. The most encouraging one is that the delay lines are easy to align. If the reentrant condition is satisfied, namely that the input and output beams pass through the same hole, the delay line behaves as though the beam is reflected by the back of the front surface of the mirror which has the coupling hole in it. The position of the output beam is independent of the transverse position and angle of the far mirror as long as the beam pattern does not spill off of the mirrors. As is discussed in appendix 2, (if the reentrant condition is satisfied) the time delay of the beam in the cavity is insensitive in first order to transverse motions and rotations of the far mirror.

The mirrors in the prototype antenna are 4 inches in diameter, have a radius of 9 meters, a reflectivity of 99.5% at 5145A and 6328A and are good to 1/10 of a wavelength over their entire surface. The coupling hole has a diameter of 1.5mm.

The design of the suspensions for the antenna masses has defied a simple, elegant and economical solution. The suspensions have to satisfy several conditions. First they must have a high Q to reduce the coupling to thermal fluctuations. Second they must provide isolation from ground and acoustic noise. What makes the problem difficult is the inevitable collection of normal modes of motion of a mechanical system which cross-couple and by parametric conversion transfer energy between each other. In other words, the isolation calculated for a long period suspension

is never realized in practice because the suspension structure has its own resonances that couple into the principle mode of the suspension. This is a problem that has long been recognized in the design of seismometers and gravimeters[17]. A rule of thumb to minimize problems in suspensions is to keep them simple and to force the resonances of the structural members toward high frequencies.

A possible answer to the suspension problem is to use a diamagnetic superconducting suspension or other field suspension such as servoed electrostatic or magnetic supports. We have made analyses of such systems and in fact constructed a prototype electrostatic suspension. However, for a first attempt at testing the design of the entire antenna, it seems prudent to make an imperfect compromise which has the virtue of simplicity.

The masses are 10kg aluminium blocks suspended as pendula by 4mm diameter fused quartz rods 1 meter long. The fundamental period of the suspension is 2 seconds and has a Q in excess of 10^6. The Q is determined by the internal losses in the quartz but only 5% of the energy of the oscillator is stored in the quartz. The remainder is stored in the gravitational field of the earth, so that the total Q is higher than the internal Q of quartz. The principle problem associated with this suspension is the normal modes of vibration of the quartz rod which occur at approximately 250Hz intervals.

Since the interferometer is insensitive to transverse motion and rotation of the far mirrors, the isolation provided by the suspension is most critical for motion along the lengths of the interferometer arms.

For diagnostic purposes as well as to measure the ground noise contribution to the antenna output, each of the suspended

masses is the inertial member of a horizontal seismometer. The motion of the ground relative to the antenna masses is measured by using capacitive displacement transducers attached to flanges in the vacuum housing. The ground noise measured by the seismometers can be subtracted from the antenna output as described in the following scheme.

The suspension is characterized by the transfer function

$$T(\omega) = x_m(\omega)/x_g(\omega)$$

where $x_m(\omega)$ is the Fourier component of the displacement of the suspended mass in inertial space when driven by a ground motion $x_g(\omega)$, also referred to inertial space. $x_g(\omega)$ is composed of seismic noise as well as the motion of the earth induced by the gravity wave. The interferometer measures the displacement of the masses relative to each other. The relative motion of the masses, $\Delta x_m(\omega)$ is

$$\Delta x_m(\omega) = \Delta x_{GW}(\omega) + T_1(\omega) x_{g1}(\omega) - T_2(\omega) x_{g2}(\omega)$$

where $\Delta x_{GW}(\omega)$ is the motion due to the gravitational wave and the subscripts 1 and 2 refer to the two suspensions involved in a single arm of the interferometer. The seismometer measures the motion of the earth relative to the position of of the suspended mass. At one end of the interferometer arm the seismometer output is

$$\Delta x_{R1}(\omega) = \frac{\Delta x_{GW}(\omega)}{2} + (T_1(\omega) - 1)\, x_{g1}(\omega)$$

while at the other end it is

$$\Delta x_{R2}(\omega) = -\frac{\Delta x_{GW}(\omega)}{2} + (T_2(\omega) - 1) x_{g2}(\omega)$$

The contribution due to the gravitational wave in terms of the measured quantities is given by

$$\Delta x_{GW} = \frac{\Delta x_m (T_1 - 1)(T_2 - 1) + \Delta x_{R_2} T_2 (T_1 - 1) - \Delta x_{R_1} T_1 (T_2 - 1)}{[\,1 - 1/2(T_1 + T_2)\,]}$$

For T_1 and $T_2 \ll 1$

$$\Delta x_{GW} = \Delta x_m + \Delta x_{R_1} T_1 - \Delta x_{R_2} T_2$$

The ground noise subtraction scheme looks promising if the suspension transfer functions are small, in other words, there is already substantial isolation of the ground motion and the non-linearities thatmay make the transfer functions amplitude dependent are small as well.

Noise Sources in the Antenna

The power spectrum of the noise from various sources in an antenna of the design shown in Figure 1 is estimated below. The power spectra are given in equivalent displacements squared per unit frequency interval.

1) Amplitude Noise in the Laser Output Power

The ability tomeasure the motion of an interferometer fringe is limited by the fluctuations in amplitude of the photo current. A fundamental limit to the amplitude noise in a laser output is the shot noise in the arrival rate of the photons, as well as the noise generated in the stochastic process of detection. At bestalaser can exhibit Poisson amplitude noise. This limit has been approached in single mode gas lasers that are free of plasma oscillations and in which the gain in the amplifying medium at the frequency of the oscillating optical line is saturated.

The equivalent spectral noise displacement squared per unit frequency interval in an interferometer of the design in Figure 1 illuminated by a Poisson noise limited laser and using optimal signal processing is given by

$$x^2(f) \geq \frac{hc\lambda}{\pi^2 \varepsilon P b^2 e^{-(b-1)(1-R)}}$$

h is Planck's constant, c the velocity of light, λ the wavelength of the laser light, ε the quantum efficiency of the photodetector, P the total laser output power, b the number of beams in each interferometer arm, and R the reflectivity of the spherical mirrors. The expression has a minimum value for

$$b = 2/(1 - R)$$

As an example, for a 1/2 watt laser at 5000 Å and a mirror reflectivity of 99.5% using a photodetector with a 50% quantum efficiency, the minimum value of the spectral noise power is

$$x^2(f) \geq 2 \times 10^{-32} \text{ cm}^2/\text{Hz}$$

2) Laser Phase Noise or Frequency Instability

Phase instability of the laser is transformed into displacement noise in an unequal path length interferometer. In an ideal laser the phase noise is produced by spontaneous emission which adds photons of random phase to the coherent laser radiation field. The laser phase performs a random walk in angle around the noise-free phase angle given by $\phi_o = \omega_o t$. The variance in the phase grows as $(\overline{\Delta\phi})^2 = t/st_c$ where s is the number of photons in the laser mode, t_c the laser cavity storage time and t the observation time. This phase fluctuation translates

into an oscillating frequency width of the laser given by

$$\delta = \frac{1}{4\pi t_c s}$$

Armstrong (18) has made an analysis of the spectral power distribution in the output of a two-beam interferometer illuminated by a light source in which the phase noise has a Gaussian distribution in time. Using his results, the equivalent power spectrum of displacement squared per unit frequency in the interferometer is given by

$$x^2(f) = \frac{16}{3} \frac{\lambda^2 \delta^2 \tau^3}{b^2}$$

in the case where $f\tau << 1$ and $\delta\tau << 1$. τ is the difference in light travel time between the two paths in the interferometer.

The main reason for using a Michelson interferometer in the gravity antenna is that τ can be made small, if necessary equal to zero, so that one does not have to make excessive demands on the laser frequency stability. In most lasers δ is much larger than that due to spontaneous emission, especially for large τ. However, for small τ, δ does approach the theoretical limit. In a typical case δ might be of the order of 10 Hz and τ approximately 10^{-9} seconds, which gives

$$x^2(f) \leq 2 \times 10^{-38} \text{ cm}^2/\text{Hz}$$

3) Mechanical Thermal Noise in the Antenna

Mechanical thermal noise enters the antenna in two ways. First there is a thermal motion of the center of mass of the masses on the horizontal suspensions and second there is thermal excitation of the internal normal modes of the masses about the

center of the mass. Both types of thermal excitation can be handled with the same technique. The thermal noise is modeled by assuming that the mechanical system is driven by a stochastic driving force with a spectral power density given by

$$F^2(f) = 4kT\alpha \qquad \text{dynes}^2/\text{Hz}$$

where k is Boltzmann's constant, T the absolute temperature of the damping medium and α the damping coefficient. α can be expressed in terms of the Q, the resonant frequency ω_o of the mechanical system and the mass

$$\alpha = m\omega_o/Q$$

The spectral power density of the displacement squared due to the stochastic driving force on a harmonic oscillator is

$$x^2(f) = \frac{1}{m^2\omega_o^4} \quad \frac{1}{(1 - z^2)^2 + z^2/Q^2} \quad \frac{4kT\omega_o m}{Q}$$

where

$$z = \omega/\omega_o$$

The seismometer suspension should have a resonant frequency much smaller than the frequency of the gravitational wave to be detected; in this case $z >> 1$ and $Q >> 1$, giving

$$x^2(f) = 4 \frac{\omega_o}{\omega^4} \frac{kT}{mQ}$$

On the other hand, the lowest normal mode frequencies of the internal motions of the masses including the mirrors and the other suspended optical components should be higher than

the gravitational wave frequency. Some care has to be taken to make the entire suspended optical system on each seismometer mount as rigid as possible. For the internal motions $z << 1$ and $Q >> 1$, so that

$$x^2(f) = \frac{4kT}{\omega_o^3 mQ}$$

If the internal Q is 10^5, the mass 10 kg, and the lowest frequency resonance in the mass 10 kHz, the thermal noise due to internal motions at room temperature for frequencies less than 10 kHz is

$$x^2(f) \sim 10^{-35} \ \text{cm}^2/\text{Hz}$$

The thermal noise due to center of mass motion on the suspension for a $Q \sim 10^6$ and a resonance frequency of 5×10^{-1} Hz becomes

$$x^2(f) \sim \frac{10^{-25}}{f^4} \ \text{cm}^2/\text{Hz}$$

for frequencies larger than the resonance frequency of the suspension.

4) Radiation Pressure Noise due to the Laser Light

Fluctuations in the output power of the laser can drive the suspended masses through the radiation pressure of light. In principle if the two arms of the interferometer are completely symmetric, both mechanically and optically, the interferometer output is insensitive to these fluctuations. Since complete symmetry is hard to achieve, this noise source must still be considered. An interesting point in pondering

this noise is that although one might find a high modulation frequency for the servo system where the laser displays Poisson noise, it is the spectral power density of the fluctuations in the laser output at the lower frequency of the gravitational wave which excite the antenna. In other words, if this is a serious noise source the laser has to have amplitude stability over a wide range of frequencies.

The radiation pressure noise can be treated in the same manner as the thermal noise. If the laser does display Poisson noise, the spectral power density of a stochastic radiation pressure force on one mirror is

$$F^2_{rad}(f) = \frac{4bhP}{\lambda c} \quad \text{dynes}^2/\text{Hz}$$

b is the number of beams in each interferometer arm and P the average total laser power. Using the same sample parameters for the suspension as in the calculation of the thermal noise, and those for the laser in the discussion of the amplitude noise, the ratio

$$\frac{F^2_{rad}(f)}{F^2_{thermal}(f)} \sim 5 \times 10^{-9}$$

5) Seismic Noise

If the antenna masses were firmly attached to the ground, the seismic noise, both through horizontal and tilt motions of the ground, would be larger than any of the other noise sources considered so far. The seismic noise on the earth at frequencies higher than 5 Hz has been studied by several investigators[19,20,21,22] at various locations both on the surface and at different depths.

In areas far from human industrial activity and traffic, the high frequency noise can be characterized by a stationary random process. The noise at the surface appears higher than at depths of 1 km or more; however, an unambiguous determination of whether the high frequency noise is due to Rayleigh or body waves has not been carried out. Measurements made in a zinc mine at Ogdensburg, New Jersey,[19] at a depth of about 1/2 km and in Jamestown, California[22] yield the smallest published values of seismic noise. In the region between 10 to 100 Hz, the power spectrum is approximated by

$$x_\ell^2(f) \sim \frac{3 \times 10^{-14}}{f^4} \text{ cm}^2/\text{Hz}$$

The spectrum has not been measured at frequencies higher than 100 Hz; however, it is not expected to decrease more slowly with frequency at higher frequencies.

By mounting the antenna masses on horizontal seismometer suspensions, the seismic noise entering the interferometer is substantially reduced. The isolation provided by a single degree of freedom suspension is given by

$$\left|\frac{x_m(f)}{x_\ell(f)}\right|^2 = \frac{[\,(1 - z^2) + (2/Q)^2\,]^2 + (z^3/Q)^2}{[\,(1 - z^2)^2 + (z/Q)^2\,]^2}$$

where $z = f/f_o$, and f_o is the resonant frequency of the suspension. $x_m(f)$ is the displacement of an antenna mass at frequency f relative to an inertial frame; $x_\ell(f)$ is the motion of the earth measured in the same reference frame.

At frequencies for which $z >> 1$, the isolation ratio is

$$\left|\frac{x_m(f)}{x_\ell(f)}\right|^2 \sim \left(\frac{f_o}{f}\right)^4 + \left(\frac{f_o}{f}\right)^2 \frac{1}{Q^2}$$

For the sample suspension parameters given previously, the estimated seismic noise entering the antenna becomes

$$x^2(f) > \frac{2 \times 10^{-14}}{f^8} \text{ cm}^2/\text{Hz} \quad 10 < f < 10 \text{ kHz}$$

At frequencies higher than 180 Hz, the seismic noise is smaller than the Poisson noise due to the laser amplitude fluctuations. If the ground noise subtraction scheme described earlier can be made to work to a precision of 1%, the laser noise remains dominant down to 50 Hz.

6) Thermal Gradient Noise

Thermal gradients in the chamber housing the suspension produce differential pressures on the suspended mass through the residual gas molecules. The largest unbalanced heat input into the system occurs at the interferometer mirror where after multiple reflections approximately 1/10 of the laser power will be absorbed.

The excess pressure on the mirror surface is approximately

$$p \sim nk\Delta T$$

where n is the number of gas molecules per cc, k Boltzmann's constant and ΔT the difference in temperature between the mirror surface and the rest of the chamber. The fluctuations in ΔT can be adequately calculated by solving the one-dimensional problem of thermal diffusion from the surface into the body of the mirror and the associated antenna mass which are assumed to be at a constant temperature.

The mirror surface temperature fluctuations T(f), driven by incident intensity fluctuations I(f), is given by

$$T(f) = \frac{\Delta I(f)}{4\varepsilon\sigma T_o^3 + (\pi c_v \rho k_t)^{1/2} f^{1/2}}$$

The first term in the denominator is the radiation from the surface; ε is the emissivity, σ the Stefan-Boltzmann constant, and T_o the ambient temperature. The second term is due to thermal diffusion from the surface into the interior; c_v is the specific heat, ρ the density and k_t the thermal conductivity of the mirror.

If the laser exhibits Poisson noise the spectral force density on the antenna mass becomes

$$F^2(f) = \frac{2(nk)^2}{f(\pi c_v \rho k_t)} \quad \frac{hc}{\lambda} \bar{P} \quad \text{dynes}^2/\text{Hz}$$

Radiation is neglected as it is much smaller than the thermal diffusion. Using the following parameters for glass, $c_v \sim 10^6$ ergs/sec cm ^oK, an average laser power of 1/2 watt and a vacuum of 1×10^{-8} mm Hg, the ratio between the thermal gradient noise to the thermal noise to the thermal noise forces in the sample suspension is

$$\frac{F^2_{T,G}(f)}{F^2_{th}(f)} \sim \frac{1}{f} 10^{-15}$$

7) Cosmic Ray Noise

The principal component of the high energy particle background both below and on the earth's surface are muons with kinetic energies larger than 0.1 Bev.[23] A muon that passes through or stops in one of the antenna masses imparts momentum to the mass, resulting in a displacement given by

$$\Delta x = \frac{\Delta E \cos \theta}{m \omega_o c}$$

ΔE is the energy loss of the muon in the antenna mass, θ the angle between the displacement and the incident muon momentum, m the antenna mass and ω_o the suspension resonant frequency.

The energy loss of muons in matter is almost entirely through electromagnetic interactions so that the energy loss per column density, k(E), is virtually constant with energy for relativistic muons. A 10^{-1} Bev muon loses 3 Mev/gm/cm^2, while a 10^4 Bev muon loses $\sim$ 30 Mev/gm/cm^2.

The vertical flux of muons at sea level with an energy greater than 10^{-1} Bev is approximately 10^{-2} particles/cm^2 sec steradian. For energies larger than 10 Bev, the intergrated flux varies as $\sim 10^{-1}/E^2$(Bev).

Since the flux falls off steeply with energy and the energy loss is almost independent of energy, the bulk of the muon events will impart the same momentum to the suspension. Using the following sample suspension parameters, m $\sim 10^4$ grams, $f_o \sim 5 \times 10^{-1}$ Hz, $\rho \sim 3$ and typical linear dimensions $\sim$ 10 cm, the average energy loss per muon becomes $\sim 10^{-1}$Bev. At sea level the antenna mass might experience impulsive displacements $\sim 10^{-18}$ cm occurring at an average rate of once per second. An event due to the passage of a 10^4 Bev muon results in a displacement of 10^{-17} cm at a rate of once per year.

Although the shape of the antenna mass can be designed to somewhat reduce the effect and frequency of muon interactions, especially by taking advantage of the anisotropy of the muon flux, the best way of reducing the noise is to place the antenna masses underground. The pulse rate at depths of 20 meters, 200 meters, and 2 km is approximately 3×10^{-2}, 10^{-4}, 10^{-9} pulses/sec.

If the antenna output is measured over times that include many muon pulses, as would be the case in a search for pulsar radiation, the noise can be treated as a stationary distribution. Assuming that the muon events are random and for

ease of calculation that the magnitude of the momentum impacts is the same for all muons, the spectral power density of displacement squared of the antenna mass is

$$x^2(f) = \frac{4N(\Delta E/c)^2}{(2\pi)^4 m^2 f^4} \quad cm^2/Hz$$

for $f >> f_o$.

N is the average number of pulses per second, $\Delta E/c$ the momentum imparted to the mass per pulse, and m the antenna mass. For the sample suspension parameters at sea level

$$x^2(f) \sim 10^{-40}/f^4 \quad cm^2/Hz$$

8) Gravitational Gradient Noise

The antenna is sensitive to gravitational field gradients -- differential gravitational forces exerted on the masses of defining the ends of the interferometer arms. No data are available concerning the naturally occurring high frequency gravitational gradients on or near the surface of the earth. There are two effects which can make gravitational gradient noise; first, time dependent density variations in both the atmosphere and the ground and second, motions of existing inhomogeneities in the mass distribution around the antenna.

An estimate for the two effects can be made with a crude model. Assume that one of the antenna masses is at the boundary of a volume that has a fluctuating density. The amount of mass that can partake in a coherent density fluctuation at a frequency f and exert a force on the mass is roughly that included in a sphere with a radius equal to half the acoustic wavelength, λ, in the ground. The fluctuating gravitational force on the mass is

$$\frac{F_g(f)}{m} \sim \frac{2}{3} \pi \lambda \Delta\rho(f) G$$

where $\Delta\rho(f)$ is the density fluctuation at frequency f and G the Newtonian gravitational constant. The density fluctuations driven by ground noise in the sphere are

$$\rho(f) = 3\langle\rho\rangle \frac{x_\varepsilon(f)}{\lambda}$$

where $\langle\rho\rangle$ is the average density of the ground and $x_\varepsilon(f)$ the ground noise displacement. If f is larger than the resonant frequency of the suspension, the ratio of the suspension, the ratio of the displacement squared of the mass to that of the ground motion is given by

$$\frac{x_m^2(f)}{x_e^2(f)} = \left[\frac{\langle\rho\rangle G}{2\pi f^2}\right]^2$$

For the earth, this isolation factor is

$$\frac{x_m^2(f)}{x_e^2(f)} \sim \frac{10^{-14}}{f^4}$$

which is much smaller than the isolation factor for the attenuation of direct ground motion by the sample suspension.

A comparable approach can be used in estimating the effect of motions of inhomogeneities in the matter distribution around the antenna which are driven by ground noise. Assuming the extreme case of a complete inhomogeneity, for example, an atmosphere ground interface, the mass that partakes in a coherent motion x(f) could be $m \sim \lambda^3\langle\rho\rangle$. The fluctuating force on the nearest antenna becomes

$$\frac{F_g(f)}{m} = \frac{2}{3}\pi G\langle\rho\rangle x(f)$$

The isolation factor is

$$\frac{x_m^2(f)}{x_e^2(f)} \sim \left[\frac{G<\rho>}{6\pi f^2}\right]^2$$

which is comparable to the isolation factor due to density fluctuations. These factors become smaller if the distance between the masses is smaller than λ.

9) Electric and Magnetic Field Noise

Electric fields in dielectric-free conducting vacuum chambers are typically 10^{-3} volts/cm. These fields are due to variations in the work function of surfaces and occur even when all the surfaces in a system are constructed of the same material, since the work function of one crystal face is different than that of another. Temporal fluctuations in these fields are caused by impurity migrations and variations in absorbed gas layers. Little is known about the correlation time of these fluctuations except that at room temperature it seems to be longer than a few seconds and at cryogenic temperatures it is possible to keep the fields constant to better than 10^{-2} volts/cm for several hours.[24]

The electric force on a suspended antenna mass is

$$F_e \sim \frac{1}{4\pi} \varepsilon^2 A$$

where A is the exposed antenna surface and ε the fluctuating electric field at the surface. Assuming that the power spectrum of the field fluctuations is similar to that of the flicker effect in vacuum tubes or the surface effects in semiconductors, which are both due to large scale but slow changes in the

surface properties of materials, the electric force power spectrum might be represented by

$$F_e^2(f) \sim \frac{\frac{2}{\pi}\langle F_e^2\rangle \, 1/\tau_o}{(1/\tau_o)^2 + (2\pi f)^2}$$

τ_o is the correlation time of the fluctuations and $\langle F_e^2\rangle$ is the average electric force squared.

If the gravitational wave frequency is much larger than $1/\tau_o$ and also higher than the resonant frequency of the suspension, the power spectrum of the displacements squared becomes

$$x^2(f) = \frac{\langle \varepsilon^4 \rangle A^2}{32\pi^6 m^2 \tau_o f^4} \quad cm^2/Hz$$

For $m \sim 10^4$ gm, $A \sim 10^2$, $\varepsilon \sim 10^{-5}$ stat volts/cm and $\tau_o \sim 1$ sec,

$$x^2(f) \sim 10^{-38}/f^4 \quad cm^2/Hz$$

Although this noise is a good deal less than that due to the Poisson noise of the laser, some care has to be taken to electrostatically shield the mirror surfaces, which are dielectrics.

Geomagnetic storms due to ionospheric currents driven by the solar wind and cosmic rays create fluctuating magnetic fields at the earth's surface. The smoothed power spectrum of the magnetic field fluctuations in mid-latitude regions at frequencies greater than 10^{-3} Hz is approximately

$$B^2(f) \sim B_o^2/f^2 \quad gauss^2/Hz$$

with $B_o \sim 3 \times 10^{-8}$ gauss.[25] Large pulses with amplitudes $\sim 5 \times 10^{-3}$ gauss are observed occasionally; the rise time of these pulses is of the order of minutes.[26]

Fluctuating magnetic fields interact with the antenna mass primarily through eddy currents induced in it or, if it is constructed of insulating material, in the conducting coating around it required to prevent charge buildup. The interaction, especially at low frequencies, can also take place through ferromagnetic impurities in nonmagnetic materials. Magnetic field gradients cause center of mass motions of the suspended mass. Internal motions are excited by magnetic pressures if the skin depth is smaller than the dimensions of the antenna mass.

An extreme model would be to assume that the fluctuating magnetic fields are completely excluded by the antenna mass and that the field changes over the dimensions of the mass are equal to the fields. The magnetic forces are

$$F_m = \frac{1}{4\pi} B^2 A$$

The power spectrum for center of mass motions, if $f >> f_o$, becomes

$$x^2(f) = \frac{A^2 B_o^4}{16\pi^3 m^2 f^4} \quad cm^2/Hz$$

For the sample suspension using the smoothed power spectrum of magnetic field fluctuations,

$$x^2(f) \sim 10^{-36}/f^4 \quad cm^2/Hz$$

The displacements due to internal motions driven by magnetic pressures at frequencies smaller than the internal

resonant frequency, $f_{o_{int}}$, are given by

$$x^2(f) = \frac{A^2 B_o^4}{16\pi^3 m^2 f_{o_{int}}^2 f^2} \quad cm^2/Hz$$

Although the disturbances due to the smoothed power spectrum do not appear troublesome relative to the other noise sources, the occasional large magnetic pulses will require that both conducting and high μ magnetic shields be placed around the antenna masses.*

---

* It is not inconceivable that Weber's coincident events may be caused by pulses in geomagnetic storms, if his conducting shielding is inadequate. It would require a pulse of 10^{-2} gauss with a rise time $\sim 10^{-3}$ seconds to distort his bars by $\Delta\ell/\ell \sim 10^{-16}$. M. Gordon has measured naturally occurring pulses of this length and amplitude as part of senior thesis project in physics at M.I.T.

The Detection of Gravitational Radiation By a Broad-Band Interferometric Antenna

The fundamental limit for the detection of gravitational radiation by an intraferometric antenna is determined by the Poisson amplitude noise of the laser and photodetection process. It appears that this limit can be reached in the prototype antenna at frequencies greater than 150 Hz. The minimum detectable gravitational radiation spectral intensity is

$$I_{g_{min}}(f) = \left(\frac{hc^4}{\pi G}\right)\left(\frac{\lambda}{\eta P_o}\right)\frac{f^2}{\ell^2 b^2 c^{-(b-1)(1-R)}} = Af^2 \frac{\text{watts}}{\text{cm}^2\text{Hz}} \qquad (1)$$

where

h is Planck's constant
c velocity of light
G Newtonian gravitational constant
λ wavelength of the laser
η quantum efficiency of the photo detector
P_o output power of the laser
f frequency of the gravitational wave
ℓ length of the interferometer arms
b the number of beams per arm
R reflectivity of the cavity mirrors

The prototype 9 meter antenna has the limit

$$I_{g_{min}}(f) = 3.2 \times 10^{-6} f^2 \quad \text{watts/cm}^2\ \text{Hz}$$

for frequencies less than 200 KHz. The high frequency limit is determined by the cavity storage time which is 9 μsec.

The length or cavity storage time for the optimum antenna satisfies the condition

$$\frac{\ell b}{c} = \tau/2$$

where τ is the period of the gravitational wave. The minimum detectable spectral intensity for the optimum antenna is

$$I_{g_{min}}(f) = \left(\frac{4hc^2}{\pi G}\right)\left(\frac{\lambda}{\eta P_o}\right) \not{X}\ f^4 = Bf^4$$

For comparison, using the same laser power and photo detection efficiency as is the prototype, the minimum detectable spectral intensity would be

$$I_{g_{min}}(f) = 2.3 \times 10^{-16} f^4 \qquad \text{watts/cm}^2\text{Hz}$$

The detection limits for periodic, broad-band and impulsive sources are described separately.

I. Periodic Sources

Periodic sources of well known frequency such as pulsars and binary systems would be synchronously detected and a narrow bandwidth would be achieved by post mixer digital integration. The gravitational radiation spectrum intensity from a periodic source is a narrow line which wanders in frequency due to the Doppler effect from the varying relative motion of the Earth and source. This frequency spread can be accomodated by adjusting the frequency of the local oscillator. The minimum detectable intensity is

$$I_{min} = \frac{I_{g_{min}}(f_o)}{2t_{int}}$$

where t_{int} is the post-mixer integration time.

As an example, the upper limit of the 60.4 Hz gravitational radiation from the Crab Pulsar NP0532 incident at the Earth is estimated at 10^{-13} watts/cm^2 (Appendix 1). Using the 9 meter prototype antenna, an integration time of 3700 years would be necessary to detect this radiation with a signal-to-noise ratio of 2. A multi-pass interferometric antenna with the same parameters as the protytype antenna, but 1 km long would require 3.6 months to detect the NP0532 upper limit. A space antenna of the optimal length, 2500 km, with single pass arms would require 8.5 hours of integration. The search for gravitational radiation could be extended to lower frequencies to include slower pulsars and binary star systems.

II. Broad-band sources

A search for broad-band gravitational radiation from discrete astronomical sources is carried out with the interferometric antenna used as a gravitational radiation radiometer and using the Earth's rotation as a modulator. If there is a discrete source of broad-band gravitational radiation, the detected signal will be a maximum each time one of the interferometer arms is perpendicular to the line joining the Earth and the source. A detection scheme for this process is shown in Figure 3. The antenna output is square-law detected and then cross-correlated with an oscillator which has a period of 1/4 of a sidereal day. In order to detect radiation from sources lying in any quadrant of the sky, the antenna output is also cross-correlated with a 90° phase-shifted output of the oscillator.

The minimum detectable signal is calculated by using the

effective noise bandwidth of the signal processing given by

$$\Delta f = \left(\frac{\Delta f_{ant}}{2t_{int}}\right)^{1/2}$$

where Δf_{ant} is the bandwidth of the antenna and post-detection filtering, and t_{int} is the observing time. The gravitational radiation signal appears as a component with a period of 1/4 of the sidereal day.

The minimum detectable signal depends on the nature of the source spectrum. If the source has a flat spectrum over the bandwidth of the antenna, the minimum detectable spectral intensity is

$$I_{g_{min}}(f) = A \left(\frac{f_h f_l}{\Delta f_{ant}}\right)^{1/2} \left(\frac{1}{2t_{int}}\right)^{1/2} \quad \text{watts/cm}^2\text{Hz}$$

where f_l and f_h are the low and high frequency cut-offs of the antenna and A is defined in equation 1 of this section.

As an example, if one extends a search from 100 Hz to 1 KHz using the 9 meter prototype antenna, the minimum detectable intensity (S/N = 2/1) after 1 month of integration is 1×10^{-5} watts/cm^{2}Hz.

If the source really had a flat spectrum, it would be best to use as low a frequency and as narrow a bandwidth as possible within the constraints that the antenna be Poisson noise limited.

If the source spectrum is a power law such as a thermal spectrum

$$I(f) = \alpha f^2,$$

the minimum detectable α, which can be related to an antenna

brightness temperature, is

$$\alpha_{min} = A \left(\frac{\Delta f_{int}}{\Delta f_{ant}}\right)^{1/2} = A \frac{1}{(2t_{int}\Delta f_{ant})}^{1/2}$$

In terms of an antenna brightness temperature

$$T_{ant_{min}} = \frac{\alpha_{min} c^2}{2k}$$

Using the maximum bandwidth in the present prototype antenna design of 200 KHz, and an integration time of 1 month,

$$\alpha_{min} \sim 3 \times 10^{-12} \quad \text{watts/cm}^2\text{Hz}^3$$

Although this may appear to be a small number, it corresponds to an appallingly high temperature of $T_{ant} \sim 10^{32}$°k. A truly thermal process will most likely not be detected with this antenna.

III. Impulsive Sources

The detection of impulsive events is difficult to analyze in detail because the sensitivity of the antenna depends somewhat on the shape of the pulse and the signal processing. We consider a pulse which lasts for a time t and has a maximum strain amplitude $\Delta\ell/\ell$. It is assumed that the pulse does not oscillate many times and that the time dependent Riemann tensor has zero mean. Aside from numerical factors of order unity which depend on the detailed shape of the pulse, the gravitational radiation energy surface density (Joules/cm^2) that passes through the antenna is approximately

$$E/A \sim \frac{c^3}{8\pi G} \frac{\left(\Delta\ell/\ell\right)^2}{t}$$

The criterion for detectability is that pulse induced strain in the antenna exceed the noise induced strain. The optimal post-detection filter has a time constant short enough to fully develop the pulse but long enough to integrate the Poisson noise. The optimal filter, a matched filter, has a time constant approximately equal to the length of the pulse. For a matched filter, the minimum detectable strain is given by

$$\left(\frac{\Delta\ell}{\ell}(t)\right)^2 = \frac{hc\lambda}{\pi^2 \eta P_o b^2 \ell^2 e^{-(b-1)(1-R)}} \frac{1}{t}$$

and the minimum detectable pulse surface energy density is

$$\left[E/A\right]_{min} = \frac{c^3}{8\pi G}\left(\frac{\Delta\ell(t)}{\ell}\right)^2 \frac{1}{t} = 8\times10^{36}\left(\frac{\Delta\ell}{\ell}\right)^2_{\nu} \frac{1}{t^2} = \frac{8\times10^{-2}}{t^2}\ \text{erg/cm}^2$$

$= 8\times10^{4}\ \text{erg/km}^2 \longrightarrow 8\ \text{erg/m}^2$

For the prototype antenna this is

$$\left[E/A\right]_{min} = \frac{4\times10^{-8}}{t^2}\ \text{Joules/cm}^2$$

Comparison of the prototype interferometric antenna with existing acoustically coupled bar antennas

The table below summarizes the published performance of several acoustic bar gravitational antennas. The first column

gives the mass of the antenna, the second the length, the third the resonant frequency, the fourth is the post-detection bandwidth, the fifth gives the mechanical Q of the bar, the sixth column gives the pulse detection limits in terms of the minimum energy observable relative to the thermal noise in the bar. These limits are expressed as minimum detectable strain amplitudes in the seventh column. The eighth column gives the minimum detectable energy surface density which is for pulses that last approximately the period of the bar. The last column gives the minimum observable spectral intensity if square-law detected and integrated for one second. The last two rows give two examples using the prototype interferometric antenna. The first example shows the estimated performance if the antenna has post-detection filtering to match Tyson's antenna. The second example is an estimate of the performance of the prototype antenna as a broad-band instrument at the lowest frequencies where Poisson noise is still expected to dominate.

The minimum observable spectral intensity of broad-band gravitational radiation that can be detected in an acoustically coupled detectors has not been discussed in the literature. In the calculations used to generate the last column of the table, it is assumed that the signal processing is done as in figure 3; however, at a modulation rate rate of 1/2 the sidereal period and it is also assumed that the dominant noise in the system is the thermal noise in the acoustically coupled structure. For these conditions, the minimum detectable gravitational spectral intensity in the vicinity of the structures resonance frequency is given by

$$I(\omega_o) > \frac{c^3 KT}{\pi G \omega_o^{3/2} l^2 MQ^{1/2} t_{int}^{1/2}}$$

Table 1

Experiment	mass Kg	length cm	Center freq. kHz	Bandwidth Hz	Q	kT_{limit}	$\left(\frac{\Delta\ell}{\ell}\right)_{min}$	E/A Joules/cm^2	$I_g(fo)$ watts/cm^{2}Hz	$\left(\frac{\Delta\ell}{\ell}\right)^2/Hz$
Weber[1,2,3,4]	1300	153	1.6	2	7.7×10^4	$\frac{1}{10}$	1×10^{-16}	25	.5	
Tyson[7]	3630	357	0.71	2	2.2×10^5	$\frac{1}{30}$	3.5×10^{-17}	1.4	.07	2×10^{-39}
Levine[5] Garwin	118	150	1.695	21	1.3×10^4	$\frac{1}{10}$	3.3×10^{-16}	300	13	
Drever[6]	300	155	1.1	800	2.2×10^3	$\frac{1}{50}$	1.4×10^{-16}	35	22	3×10^{-37}
Interferometric antenna Ex. 1	30	900	.71	1000	-	-	5×10^{-18}	.04	.02	
Interferometric antenna Ex. 2	30	900	.2	100	-	-	1.6×10^{-18}	4×10^{-4}	8.5×10^{-3}	

GPU = 10^{-2} Joules/cm^2 Hz = 10^5 ergs/cm^2 Hz

$$\left(\frac{\Delta\ell}{\ell}\right)^2/_{Hz} = \frac{8\pi G}{c^3}\,\frac{I_g(\nu)}{f^2} = (1.5\times10^{-39})\,\frac{I_g(\nu)}{f^2}$$

($I_g(\nu)$ in ergs/sec cm^2 Hz)

FIGURES

Figure 1

Schematic drawing of the antenna being constructed at M.I.T.

Figure 2.

Amplitude noise in a Spectra Physics Model 165 Argon Ion Laser operating in a single longitudinal mode.

Figure 3.

Detection scheme for localized broad-band sources.

Figure 1

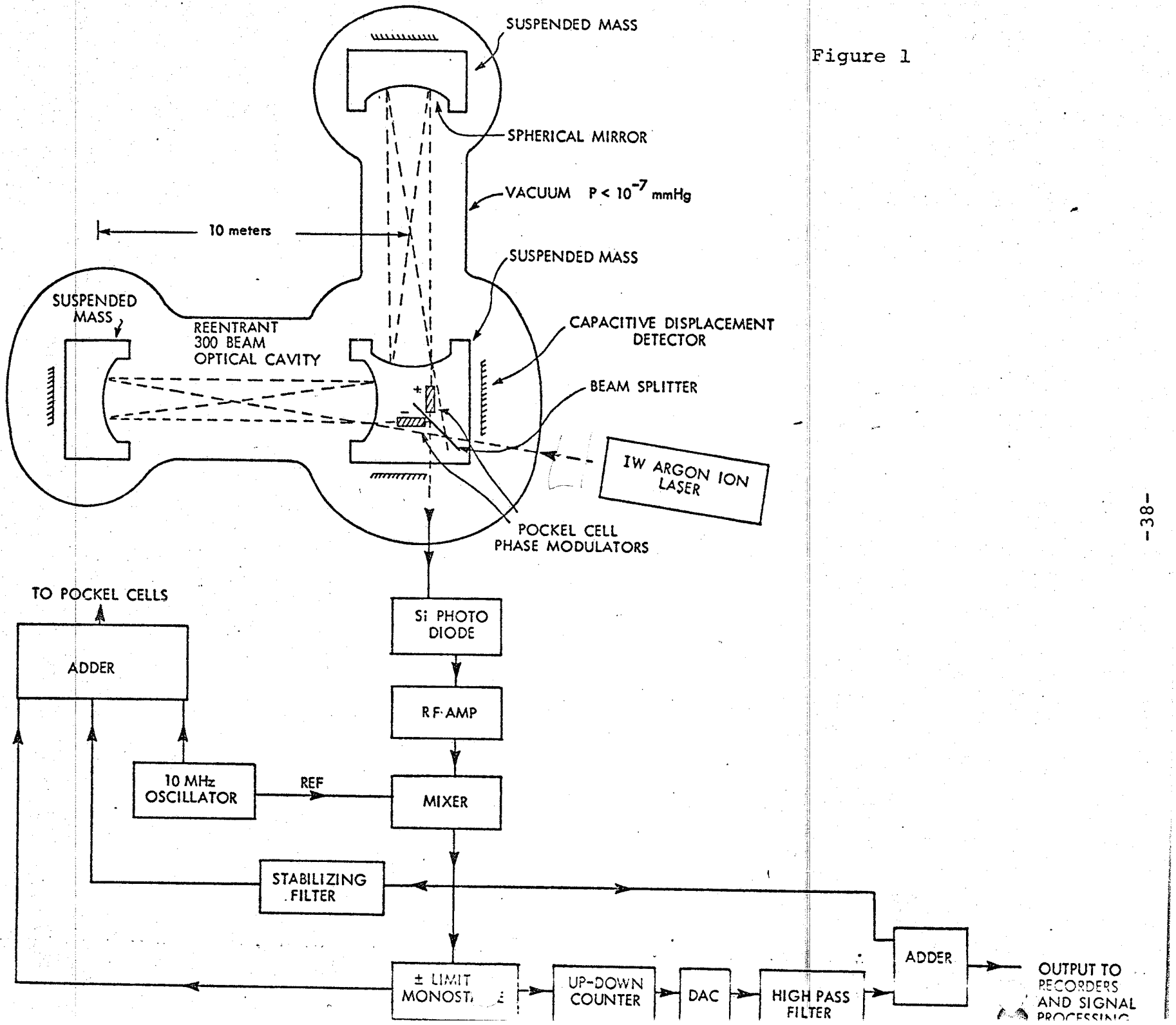
SUSPENDED MASS
SPHERICAL MIRROR
VACUUM P < 10^-7 mmHg
10 meters
SUSPENDED MASS
SUSPENDED MASS
REENTRANT 300 BEAM OPTICAL CAVITY
CAPACITIVE DISPLACEMENT DETECTOR
BEAM SPLITTER
1W ARGON ION LASER
POCKEL CELL PHASE MODULATORS
TO POCKEL CELLS
ADDER
Si PHOTO DIODE
RF AMP
10 MHz OSCILLATOR
REF
MIXER
STABILIZING FILTER
± LIMIT MONOST
UP-DOWN COUNTER
DAC
HIGH PASS FILTER
ADDER
OUTPUT TO RECORDERS AND SIGNAL PROCESSING

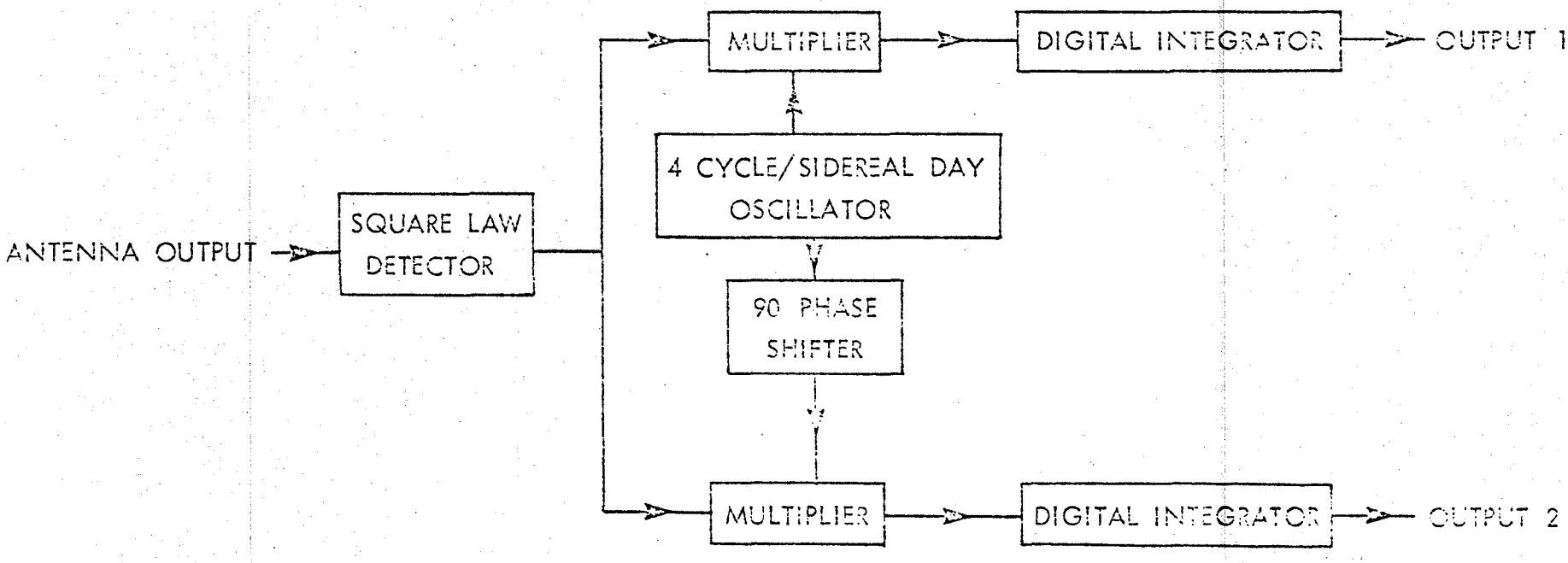
ANTENNA OUTPUT
SQUARE LAW DETECTOR
MULTIPLIER
DIGITAL INTEGRATOR
OUTPUT 1
4 CYCLE/SIDEREAL DAY OSCILLATOR
90 PHASE SHIFTER
MULTIPLIER
DIGITAL INTEGRATOR
OUTPUT 2

Figure 3

References

1. J. Weber, Phys. Rev. Letters 22, 1320 (1969).
2. J. Weber, Phys. Rev. Letters 25, 180 (1970).
3. J. Weber, Phys. Rev. 117, 306 (1960).
4. J. Weber et. al., Phys. Rev. Letters 31, 779 (1973).
5. J. L. Levine and R. L. Garwin, Phys. Rev. Letters 31, 173 (1973).
6. R. W. P. Drever et. al., Nature 246, 340 (1973).
7. J. A. Tyson, Phys. Rev. Letters 31, 326 (1973).
8. D. Douglass, report at Fifth "Cambridge" Conference on Relativity, 1974.
9. W. D. Allen, report at Fifth "Cambridge" Conference on Relativity, 1974.
10. R. L. Garwin, report at Fifth "Cambridge" Conference on Relativity, 1974.
11. A. Einstein, Sitzber. deut. Adad. Wiss. Berlin, Kl. Math. Physik u. Tech. (1916), p. 688; (1918), p. 154.
12. L. D. Landau and E. M. Lifshitz, The Classical Theory of Fields (Pergamon Press, London and New York, 1962).
13. F.A.E. Pirani, Acta Phys. Polon. 15, 389 (1956).
14. G. Blum and R. Weiss, Phys. Rev. 155, 1412 (1967).
15. G. F. Moss, L. R. Miller, and R. L. Forward, Appl. Opt. 10, 2495 (1971).
16. D. R. Herriott and H. J. Schulte, Appl. Opt. 4, 883 (1965).
17. R. Weiss and B. Block, J. Geophys. Ros. 70, 5615 (1965).
18. J. A. Armstrong, J. Opt. Soc. Am. 56, 1024 (1966).

19. B. Isacks and J. Oliver, Bull. Seismol. Soc. Am. 54, 1941 (1964).

20. G. E. Frantti, Geophys. 28, 547 (1963).

21. E. J. Douze, Bull. Seismol. Soc. Am. 57, 55 (1967).

22. T. S. Mast, J. E. Nelson and J. A. Saarloos, Ap. J. 187, L49 (1974).

23. M. G. K. Menon and P. V. Ramana Murthy, in Progress in Elementary Particle and Cosmic Ray Physics, Vol. 9 (North-Holland Publishing Co., Amsterdam, 1967).

24. F. C. Witteborn and W. M. Fairbank, Phys. Rev. Letters 19, 1049 (1967).

25. W. H. Campbell, Ann. Geophys. 22, 492 (1966).

26. T. Sato, Rep. Ionosphere Space Res. Japan 16, 295 (1962).

27. M. Gordon, Senior Thesis, Mass. Inst. of Tech. (unpublished) 1973.

APPENDIX 1

Appendix I

Astrophysical Sources of Gravitational Radiation

The astrophysical sources of gravitational radiation discussed here are collisions, pulsars, neutron stars, and binary stars. Exotic phenomena such as 10^8 $M_\odot$ black holes in the Galactic center will not be considered. Collisions between collapsed objects, or matter falling into collapsed objects could produce considerable amounts of gravitational radiation; however, it appears that direct collision is a rare occurrence. Supernovae, and the formation of neutron stars could also be strong sources of gravitational radiation but the expected mean time between events of 5 to 50 years does not make these sources very attractive. The two remaining sources of gravitational radiation, pulsars and binary stars, are believed to be continuous emitters and are probably the best candidates for future studies of gravitational radiation. Both of these sources will be difficult to observe. Pulsars emit in a favorable frequency range of 1 to 60 Hz but the strain induced at the detector is very small. Binary stars produce substantial strains at the antenna but at frequencies less than 4×10^{-4} Hz. There are undoubtedly other sources of gravitational radiation not listed in Table 2; however, it is hoped that the sources and formulas listed are representative enough to give some idea of the events which could be detected by gravitational wave antennas to be built in the near future.

To get some idea of the collision rate for collapsed objects, some estimate must be made of the number of these objects in the Galaxy. Peebles (1) notes that between ten and twenty percent of the mass in the Galaxy resides in stars of

mass greater than 2 $M_\odot$. A 2 $M_\odot$ exhausts its fuel in about 2×10^9 years and since the Galaxy is about 10^{10} years old, perhaps ten or twenty percent of the mass of the Galaxy is contained in collapsed objects. The mass of the Galaxy is about 2×10^{11} $M_\odot$ and if ten percent of this mass goes into 2 $M_\odot$ collapsed objects, then we can estimate that there are roughly 10^{10} collapsed objects in the Galaxy. Ostriker, Rees, and Silk (2) note that 10^9 neutron stars moving through the interstellar plasma could produce an X-ray flux comparable to the X-ray luminosity of the Galaxy. For the following, it will be assumed that ten percent of the stars in any region of the Galaxy are collapsed.

The total collision rate of type 1 objects onto type 2 objects in a volume V, can be estimated using

$$R = \frac{N_1 N_2}{V} \langle v_{rel} \rangle \sigma_{12}$$

for the rate and

$$\sigma_{12} = \pi (R_1+R_2)^2 \left[1 + \frac{2G(M_1+M_2)}{(R_1+R_2)\langle v_{rel} \rangle^2} \right]$$

for the direct collision cross-section. N_1 and N_2 are the number of type 1 and type 2 objects, V is the volume of the interaction region, $\langle v_{rel} \rangle$ is the average relative speed at large seperation, R is the radius and M the mass of the objects, and G is the gravitational constant. Table 1 shows the mean time between collisions for various objects in the globular cluster M92 and in the Galactic center. For M92 the central density is about 6000 stars pc^{-3}, there are about 10^5 stars and $\langle v_{rel} \rangle \simeq 5$ $kmsec^{-1}$. For the Galaxy the central density is about 10^6 stars pc^{-3}, there are about 5×10^8 stars and $\langle v_{rel} \rangle$

$\simeq$ 200 kmsec^{-1}. For the stars, we assume M = 1M$\odot$, R = 1R$\odot$ and for the collapsed objects M = 1.5M$\odot$ and R = 10km.

Table 1: Mean time between collisions

	M92	Galactic center
Stars on stars	3.4×10^6y	160y
Collapsed stars on stars	5.4×10^7y	2500y
Collapsed stars on collapsed stars	1.6×10^{13}y	7.4×10^8y

The foregoing analysis only considered collisions between free objects; however, it should be pointed out that the collision rate could be considerably larger if the collapse of multiple star systems is considered. The stars in a binary system could evolve to a neutron star and a black hole, for instance, and then spiral together. One can speculate that there are many old binary systems in the Galaxy consisting of collapsed members and that these systems are only now spiralling together in considerable numbers. With no evidence to support this speculation, we will use the rates presented in Table 1.

We can make some estimate of the mean time between large bursts of gravitational radiation from stellar collapse. The most optimistic position is to assume that every star of mass greater than 1.5M$\odot$ evolves into a neutron star or a black hole and emits a large amount of gravitational radiation in the final collapse. The rate at which stars reach the endpoint in their

evolution is estimated to be about once every five years in the Galaxy (3). Pulsars provide a lower limit to the rate of gravitational bursts. If neutron stars are formed rapidly in a stellar collapse, they will probably emit considerable amounts of gravitational radiation. Since pulsars are generally agreed to be rotating neutron stars, we can say that the neutron star formation rate is at least as large as the pulsar formation rate which is about once every 30 years (4). It is clear that some supernovae produce neutron stars, for example NP0532; however, some models of supernovae leave no star remnants behind. If we assume though, that all supernovae produce a burst of gravitational radiation, then another limit can be set on the mean time between bursts in the Galaxy. Various estimates of the supernova rate based on observations of other galaxies (5), calculations of stellar evolution (6), and radio measurements at 1GHz (7) all yield a supernova rate of one every 17 to 50 years. An estimate of the mean time between large bursts of gravitational radiation in the Galaxy is between 5 and 50 years.

TABLE 2

SOURCE	EQUATIONS + COMMENTS	AMOUNT OF GRAVITATIONAL RADIATION EMITTED	MEAN TIME BETWEEN EVENTS
eutron Star on-radial ulsations efs. 8	A neutron star could form in a highly excited and distorted state with the non-radial modes excited The power radiated and the energy stored in a mode are proportional to $\left\langle \left(\frac{\delta R^2}{R} \right) \right\rangle$ the averaged square of the relative amplitude of the star's surface. H-W refers to the Harrison-Wheeler equation of state VY refers to the Levinger-Simmons-Tsuruta-Cameron equation of state τ is the damping time for the energy in the mode		Perhaps once every 5-50 years in the Galaxy

	M/M⊙	f(kHz)	τ(sec)	-ΔE(ergs)	-dE/dt(ergs/sec)
H-W	.405	.84	6.5	7.8×10^{48}	1.2×10^{48}
H-W	.682	3.2	.1	2.8×10^{50}	2.9×10^{51}
		5.9	.14	3.6×10^{49}	2.6×10^{51}
		8.3	.65	2.6×10^{48}	3.9×10^{48}
		11.1	12	8.9×10^{46}	7.0×10^{45}
V_γ	.677	1.5	.85	5.7×10^{50}	7.0×10^{50}
		4.2	5.5	6.0×10^{48}	1.1×10^{48}
V_γ	1.954	2.7	.11	1.7×10^{52}	1.6×10^{53}
		6.7	.8	1.5×10^{52}	1.9×10^{52}
		10	1.3	5.2×10^{51}	4.0×10^{51}

SOURCE	EQUATIONS + COMMENTS	AMOUNT OF GRAVITATIONAL RADIATION EMITTED	MEAN TIME BETWEEN EVENTS
eutron Star apidly rotating n the form of a acobi ellipsoid triaxial ellipsoid) efs. 9,10,11	A neutron star could form in a highly deformed, rapidly rotating state, possibly in the form of a Jacobi ellipsoid, Chau and Srulovicz conclude that it is possible for a neutron star to assume the figure of a rotating Jacobi ellipsoid. $-\frac{dE}{dt} = \frac{32G}{125c^5} M^2 (a_1^2 - a_2^2)^2 \omega^6$ a_1, a_2, a_3 are the triaxial radii, here rotation is about a_3 axis, $a_1 a_2 a_3$ = const. $1 - a_2/a_1 \sim e^{-\tau/b}$ τ in units of $\frac{25}{18}\left(\frac{\bar{a}}{RS}\right)^3\left(\frac{\bar{a}}{c}\right)$ $\omega_m^* - \omega \sim e^{-2\tau/b}$ $b = 16.039$ $\bar{a} = (a_1 a_2 a_3)^{1/3}$ $R_s = 2GM/c^2$ $\omega_m^* = .6117(\pi G\rho)^{1/2}$ is the limiting rotation rate for the non-radiating McLaurin Ellipsoid ($a_1 = a_2$) to which the Jacobi ellipsoid evolves. note: $\omega < \omega_m^*$, the rotation rate increases but only by a small amount, 7% for the case considered here.	Assume a Jacobi ellipsoid with maximum distortion, then $\omega = .5329(\pi G\rho)^{1/2}$ $a_2/a_1 = .4322$ $a_3/a_1 = .3451$ assuming $\bar{a}$ = 20 km, M = 1M⊙ then $-\Delta E = 9 \times 10^{50}$ ergs $-dE/dt = 4 \times 10^{51}$ ergs/sec spectrum peaks around $f \simeq 320$ Hz $\tau = .23$ sec.	every 5-50 years in the Galaxy if all the pulsars are formed as Jacobi ellipsoids then at least once every 30y.

SOURCE	EQUATIONS & COMMENTS	AMOUNT OF GRAVITATIONAL RADIATION EMITTED	MEAN TIME BETWEEN EVENTS
Neutron Star Pulsar refs.12,13,14, 15	Gravitational radiation emitted: $-\frac{dE}{dt} = \frac{32}{125} G/c^5 \, M^2\omega^6 (a_2^2 - a_1^2)^2$ a_1, a_2 radii perpendicular to rotation axis, ω=pulsar rotation rate, assuming $a_2 - a_1 = \varepsilon R$ R = average radius $-\frac{dE}{dt} = \frac{128}{125} \frac{G}{c^5} M^2 \omega^6 R^4 \varepsilon^2$ spectrum is monochromatic at 2ω Assuming pulsar looses energy only by emission of electromagnetic and gravitational quadrupole radiation and that $\varepsilon \approx$ const. for recent times $-\frac{dE}{dt}_{GQ} = -\left[\left(\frac{dp}{d\tau}\right)^{-1} \frac{d^2P}{dt^2} + \frac{1}{P}\frac{dP}{dt}\right] \frac{I\omega^2}{2}$ P is pulsar period, I is moment of inertia	For NP0532, the Crab pulsar, Ostriker and Gunn assume ε constant for the entire history of the pulsar. ε is fixed by requiring that the calculated age of the pulsar agree with the known age. For NP0532: M = 1.4 $M_\odot$ R = 12km I = 1.4 $\times 10^{45}$ gm-cm^2 distance = 1700 pc P = .033s $dP/dt = 420 \times 10^{-15}$ $d^2P/dt = -100 \times 10^{-25}$ sec^{-1} then $\varepsilon = 3 \times 10^{-4}$ so $-dE/dt = 1.5 \times 10^{38}$ ergs/sec from the second derivative measurement $\frac{(-dE/dt)_{GQ}}{(-dE/dt)_{total}} = .44$ whereas Ostriker and Gunn get about 1/4 for this ratio. The second derivative of the period is rather uncertain.	Pulsars formed about once every 30 years. After formation and initial damping continuous production of gravitational radiation for about 10^6 years

SOURCE	EQUATIONS + COMMENTS	AMOUNT OF GRAVITATIONAL RADIATION EMITTED	MEAN TIME BETWEEN EVENTS
Neutron Star Pulsar starquake refs. 16	The crust of a neutron star shifts releasing energy which can be radiated away as gravitational radiation. Assume that all of the released energy goes into one of the non-radial oscillation modes of the neutron star $-\Delta E = 4\left(\frac{I\omega^2}{2}\right)\frac{\delta\omega}{\omega}$ ω = rotation frequency of the pulsar $\delta\omega$ = change in the pulsar frequency due to starquake. Taking the V_γ model with $M/M\odot$ = 1.95 from K. Thornes study and the lowest mode with a frequency of 2.6 kHz $\left\langle \frac{E}{\left(\frac{\delta R}{R}\right)^2} \right\rangle = 1.7 \times 10^{54}$ SO $-\frac{dE}{dt} = 37.6\left(\frac{I\omega^2}{2}\right)\frac{\delta\omega}{\omega}$	Assuming a pulsar radius of 10 km and $M = 1.4M\odot$ a period of .033s, $\delta\omega/\omega = 2.5 \times 10^{-9}$ from the Sept. 1969 speedup of NP0532. $-dE/dt = 1.5 \times 10^{38}$ ergs/sec $-\Delta E = 1.6 \times 10^{37}$ ergs spectrum peaks around 5.2 kHz τ = .11 sec The power output is comparable to the expected gravitational radiation at 60 Hz.	to be expected every few years from the Crab

SOURCE	EQUATIONS + COMMENTS	AMOUNT OF GRAVITATIONAL RADIATION EMITTED	MEAN TIME BETWEEN EVENTS
Particle falling radially into a Schwarzshild black hole refs. 17,18,19	A particle of mass m falls into a non-rotating black hole of mass M ($m \ll M$). $-\Delta E = .0104\ mc^2 \left(\frac{m}{M}\right)$ Spectrum peaks at a frequency $\omega = .32\ c^3/GM$ The event lasts a time $\tau \simeq 2 \times \frac{2\pi}{\omega}$	Assume a .5$M_\odot$ neutron star falls into a 5 $M_\odot$ black hole. A realistic calculation should take into account tidal disruption of the neutron star $-\Delta E = 9.4 \times 10^{51}$ ergs $-dE/dt = 9.4 \times 10^{54}$ ergs/sec spectrum peaks around 2 kHz $\tau \simeq 10^{-3}$ sec	greater than every 10^8 years at the Galactic center

SOURCE	EQUATIONS + COMMENTS	AMOUNT OF GRAVITATIONAL RADIATION EMITTED	MEAN TIME BETWEEN EVENTS
Black holes in collision Two black holes collide and coalesce refs. 20,21,22	From the paper by Gibbons and Hawking, expect a pulse of radiation which is one or two cycles of a sinusoidal wave train. From the spectrum of a particle falling into a black hole, expect the spectrum to peak around $\omega = c^3/GM$ which is essentially the orbital frequency of a photon in orbit near the Schwarzshild radius of the black hole. Expect the event to last a time $\tau \simeq \frac{2\pi}{\omega}$ The total possible energy radiated is 29.3% of the rest mass for non-rotating black holes and 50% of the rest mass for extreme Kerr black holes.	Assume two 2 $M_\odot$ non-rotating black holes $-\Delta E = 2.1 \times 10^{54}$ ergs $-dE/dt = 1.7 \times 10^{58}$ ergs/sec spectrum peaks around 8 kHz $\tau = 1.2 \times 10^{-4}$ sec	greater than once every 10^8 years, assuming 10% of the stars in the core are black holes

SOURCE	EQUATIONS + COMMENTS	AMOUNT OF GRAVITATIONAL RADIATION EMITTED	MEAN TIME BETWEEN EVENTS
Particle spiralling into a black hole refs. 23,24	Total energy radiated before the particle falls into the black hole is the binding energy of the last stable orbit. Spectrum is essentially monochromatic at twice the orbital frequency. Elliptical orbits will emit at multiples of the fundamental frequency but will quickly become circular. Typical power radiated is $-\frac{dE}{dt} \simeq \frac{32G}{5c^5}\left(\frac{mM}{m+M}\right)^2 R^4\omega^6$ and typical time is $\tau = {}^{-\Delta E}/_{-\frac{dE}{dt}}$ A) Non-rotating black hole of mass M, particle of mass m $-\Delta E = .0572mc^2 \quad \omega_{max} = (GM/R_3)^{1/2}$ $R = 6\ (2GM/c^2)$ B) Exteme Kerr black hole, particle orbiting in the same direction as black hole rotation $-\Delta E = .4226mc^2 \quad \omega_{max} = \frac{1}{2}(GM/R^3)^{1/2}$ $R = 2GM/c^2$ C) Extreme Kerr black hole, retrograde $-\Delta E = .0377mc^2 \quad \omega_{max} = 1.038(GM/R^3)^{1/2}$ $R = 9 \times (2GM/c^2)$	Realistic example difficult to calculate since tidal forces on the small mass should be taken into account. For this example assume a 1 $M_\odot$ (10km radius) neutron star spirals into a 5$M_\odot$ (14.8 km radius) black hole Roche Limit $= 2.45\left(\frac{\rho BH}{\rho NS}\right)^{1/3} \times R_{BH}$ $= 42$ km For source at Galactic center A) $-\Delta E = 1.03 \times 10^{53}$ ergs $-dE/dt = 2.6 \times 10^{53}$ ergs/sec spectrum peaks at 310 Hz, $\tau = 2.5$s B) $-\Delta E = 7.6 \times 10^{53}$ ergs $-dE/dt = 3.2 \times 10^{55}$ ergs/sec spectrum peaks at 2.3kHz C) $-\Delta E = 6.8 \times 10^{52}$ ergs $-dE/dt = 4.3 \times 10^{52}$ ergs/sec spectrum peaks at 176 Hz, $\tau = 1.6$s	greater than 10^8 years in the Galactic center

SOURCE	EQUATIONS + COMMENTS	AMOUNT OF GRAVITATIONAL RADIATION EMITTED	MIN TIME BETWEEN EVENTS
Masses in Keplerian orbits refs. 25,26,27	The maximum power radiated by Keplerian orbits (at closest approach) $-\frac{dE}{dt} = \frac{32}{5}\frac{G^4}{c^5}\frac{M_1^2 M_2^2 (M_1+M_2)}{a^5}\times \frac{(1+e)^6}{(1-e^2)^5}$ where a = semimajor axis (minimum separation is a(1-e), maximum is a(1+e)) e = eccentricity of orbit power averaged over one orbit is $-\frac{dE}{dt} = \frac{32}{5}\frac{G^4}{c^5}\frac{M_1^2 M_2^2 (M_1+M_2)}{a^5(1-e^2)^{7/2}}\times \left(1+\frac{73}{24}e^2+\frac{37}{96}e^4\right)$ for e<.2, the energy is radiated mainly at 2ω, where $\omega = \left[\frac{G(M_1+M_2)}{a^3}\right]^{1/2}$ in terms of the initial conditions, the lifetime of the system against decay by gravitational radiation is $\tau = \frac{5c^5}{256G^3}\frac{a^4}{M_1 M_2 (M_1+M_2)}$	some examples of close binary systems (e=0) star — period(days) — M1 in M⊙ — M2 — -dE/dt ergs/sec — distance pc i Boo — .268 — 1.4 — .7 — 3.6×10^{30} — 12 UV Leo — .6 — 1.4 — 1.3 — 7.2×10^{29} — 68 V Pup — 1.45 — 16.6 — 9.8 — 6.6×10^{31} — 390 YY Eri — .321 — 1.0 — 0.6 — 8.9×10^{29} — 42 SW Lac — .321 — 1.0 — 1.2 — 2.9×10^{30} — 74 WU Ma — .33 — 1.3 — .65 — 1.4×10^{30} — 67 WZ Sge — 81 min — .56 — .19 — 1.5×10^{31} — 97	

References

1. Peebles, P.J.E. (1971). General Relativity and Gravitation, 3, 63.

2. Ostriker, J.P., Rees, M.J. and Silk, J. (1970). Astrophys. Letters, 6, 179.

3. Novikov, I.D. and Zel'dovich, Ya. B. (1971). Relativistic Astrophysics, (University of Chicago Press), p. 465.

4. Gunn, J.E. and Ostriker, J.P. (1970). Ap. J., 160, 979.

5. Tammann, G.A. (1970). Astron. and Astrophys., 8, 458.

6. Stothers, R. (1963). Ap. J. 138, 1085.

7. Ilovaisky, S.A. and Lequeux, J. (1972). Astron. and Astrophys., 20, 347.

8. Thorne, K.S. (1969). Ap. J., 158, 1.

9. Chandrasekhar, S. (1970). Ap. J., 161, 571.

10. Chandrasekhar, S. (1970). Phys. Rev. Letters, 24, 611.

11. Chau, W.Y. and Srulovicz, P. (1971). Phys. Rev., D3, 1999.

12. Ostriker, J.P. and Gunn, J.E. (1969). Ap. J., 157, 1395.

13. Chau, W.Y. (1966). Ap. J., 147, 664.

14. Ferrari, A. and Ruffini, R. (1969). Ap. J., 158, L71.

15. ter Haar, D. (1972) Physics Reports, Phys. Lett. Sec. C, 3C, 57.

16. Baym, G. and Pines, W.H. (1971). Annals of Physics, 66, 816.

17. Davis, M., Ruffini, R., Press, W.H. and Price, R.H. (1971) Phys. Rev. Lett., 27, 1466.

18. Davis, M., Ruffini, R. and Tiomno, J. (1972). Phys. Rev., D5, 2932.

19. Ruffini, R. (1973). Phys. Rev., D7, 972.

20. Gibbons, G.W. and Hawking, S.W. (1971). Phys. Rev., D4, 2191.

21. Hawking, S.W. (1971). Phys. Rev. Lett., 26, 1344.

22. Gibbons, G.W. and Schutz, B.F. (1972). Mon.Not. R. astr. Soc., 159, 41P.

23. Bardeen, J.M., Press, W.H. and Teukolsky, S.A. (1972). Ap.J., 178, 347.

24. Landau, L.D. and Lifshitz, E.M. (1962). The Classical Theory of Fields, (Pergamon Press and Addison-Wesley Publishing Co. Inc.), §104.

25. Peters, P.C. and Mathews, J. (1963). Phys. Rev., 131, 435.

26. Braginskii, V.B. (1966). Sov. Phys. Usp., 8, 513.

27. Faulkner, J. (1971). Ap. J., 170, L99.

APPENDIX 2

Appendix 2 Spherical Mirror Delay Lines

The optical delay line to be discussed consists of two concave spherical mirrors having the same radius of curvature[1]. One of the mirrors has a small hole in it through which the beam enters and exists (Fig. 1). Other possible configurations use a small mirror or light pipe to deflect the beam into and out of the cavity. Slightly astigmatic mirrors have also been used to utilize more of the mirror surface and increase the total delay[2]. The purpose of this appendix is to present some of the properties of spherical-mirror optical delay lines including the stability of the cavity and the change in delay time for small rotations and translations of one of the mirrors.

In Fig. 2, two spherical mirrors have been placed in a delay line configuration with mirror B slightly rotated. There is a unique line called the optical axis of the delay line which passes through the mirrors at points labelled P_A and P_B. The optical axis is defined by the condition that the line which runs through P_A and P_B be parallel to the mirror normal at P_A and P_B. The optical properties of the cavity are invariant for rotations about the optical axis. In the paraxial ray limit ($\sin\theta \simeq 0, \cos\theta \simeq 1$) it is possible to derive an expression for the points on the mirrors where the beams are reflected. In the coordinate system defined by the optical axis

$$X_n = A\sin(n\phi+\alpha)$$

where

$$\tan\alpha = \sqrt{\frac{2R}{L} - 1} \Bigg/ \left(1 + \frac{RX_o'}{X_o}\right)$$

$$\cos\phi = 1 - L/R$$

$$A^2 = \frac{2R}{2R-L}\left[X_o^2 + LX_oX_o' + \frac{RL}{2}X_o'^2\right]$$

L is the cavity length, R is the radius of curvature of the mirrors, X_o is the entry point of the initial ray , and X_o' is the x-component of the angle that the ray makes to the optical axis. A similar expression holds for Y_n. Even n gives the position on mirror A and odd n gives the position on mirror B. If L and R are chosen such that

$2r\phi = 2m\pi$ where m is an integer and

$1 \leq m \leq r - 1$ and sm/r is not an integer for $1 \leq s \leq r-1$, then there will be r reflections on each mirror (counting the hole as a reflection) and the beam will exit through the hole in mirror A as if reflected from the back of that mirror. This is called the reentrant condition.

If mirror B is moved and the cavity length changes, the output beam will shift with respect to the hole in mirror A. We will assume that the motion of mirror B is small enough so that the beam still exits through the hole in mirror A. A rough estimate of the allowed motion of mirror B will be made in the next paragraph. Since the number of beams in the cavity is assumed constant, the change in delay time can be calculated. To a good approximation, the total beam length is just the number of beams in the cavity times the distance between points P_A and P_B in Fig. 2, and can be calculated in terms of L, R, the translation (X,Y,Z), and the rotation (θ_x,θ_y) about P_B. Denoting the delay time by t, the number of beams by N and the speed of light by c the following formulas result

$$\frac{\partial t}{\partial x} = -\frac{N}{c}\frac{x}{2R-L}, \quad \frac{\partial t}{\partial y} = -\frac{N}{c}\frac{y}{2R-L}, \quad \frac{\partial t}{\partial z} = \frac{N}{c}$$

$$\frac{\partial t}{\partial \theta_x} = \frac{N}{c}\frac{R(R-L)}{(2R-L)}\theta_x, \quad \frac{\partial t}{\partial \theta_y} = \frac{N}{c}\frac{R(R-L)}{(2R-L)}\theta_y$$

These formulas are in excellent agreement with computer calculations using the geometrical optics approximation to the delay line.

In order to estimate the allowed motion of mirror B we will assume that the reentrant condition has been satisfied and that the initial ray has been chosen so that there is a circular pattern of reflection points on each mirror. In this case ϕ is the angle between consecutive reflections (Fig. 3). The configuration is stable for small motions of mirror B if the beam continues to exit through the hole in mirror A and the number of reflections remains constant. Using the relation

$\cos\phi = 1-L/R$, the change in ϕ per reflection is

$$\delta\phi = \delta L/(R\sin\phi)$$

Stability requires that

$$N|\delta\phi|d_1 < d_2$$

where N is the number of beams, d_1 is the radius of the pattern and d_2 the radius of the hole. Substituting

$$|\delta L| < \frac{d_2}{d_1}\frac{R|\sin\phi|}{N}$$

For the cavity we plan to use R = 900cm cos ϕ ~ 0, N = 302, d_2 = .075cm d_1 = 3.81cm so

↓
3" Diam

$$|\delta L| < .06\text{cm}$$

If this $|\delta L|$ were caused by a translation transverse to the optical axis, then the translation would be of the order of 1/2cm. For a rotation the angle would be about 1/2°. We have built and tested a delay line and find that the reentrant condition remains satisfied for all movements of mirror B which keep the beam within the cavity. The output beam is not observed to move.

References:

1. D. Herriott, H. Kogelnik, and R. Kompfner, Applied Optics 3, 523 (1964).

2. D. Herriott, and H. Shulte, Applied Optics 4, 833 (1965).

Figures

Figure 1

Spherical mirrors in delay line configuration.

Figure 2

Spherical mirrors in delay line configuration with mirror B slightly rotated.

Figure 3

ϕ is the angle between consecutive reflections.

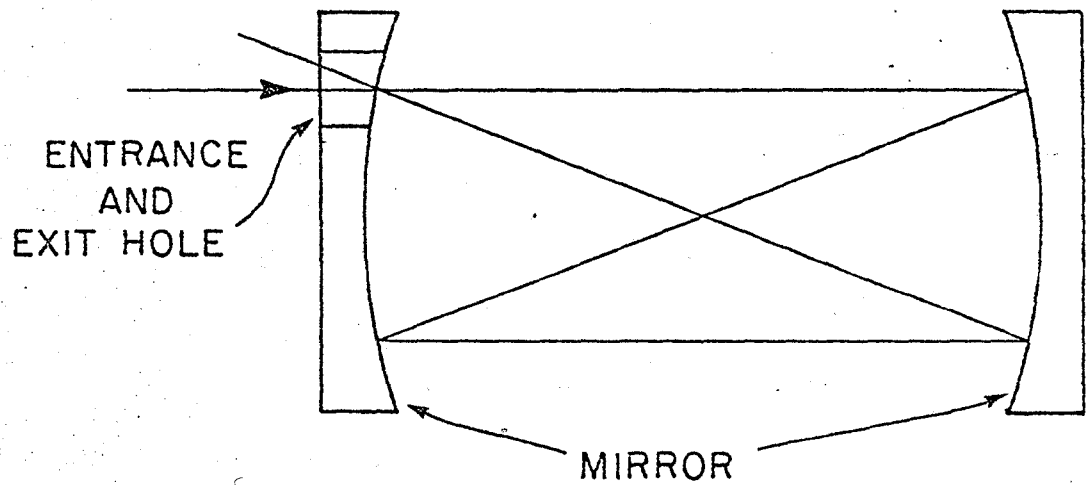

Figure 1

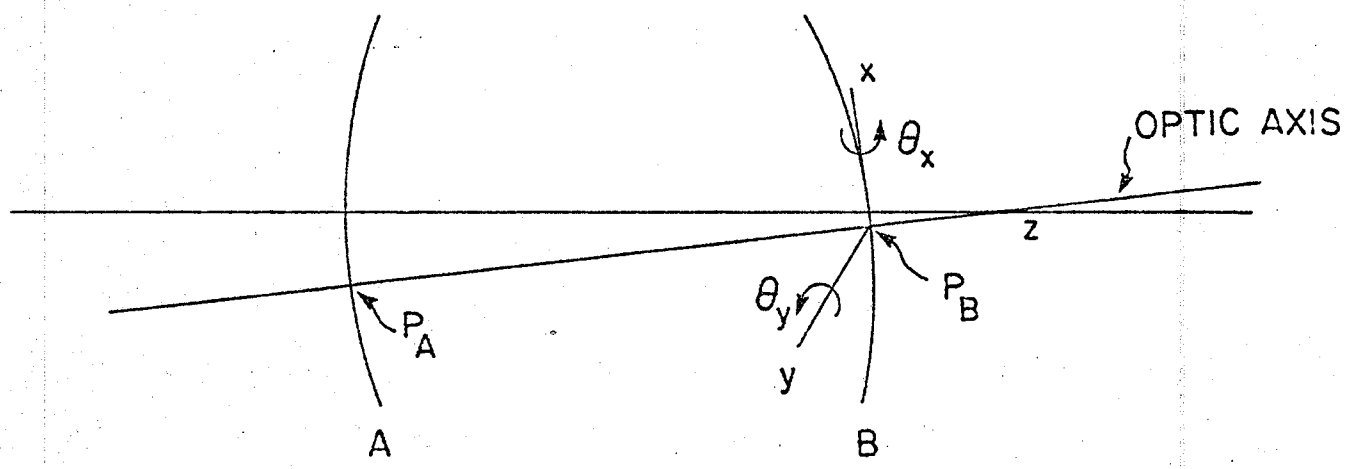

Figure 2

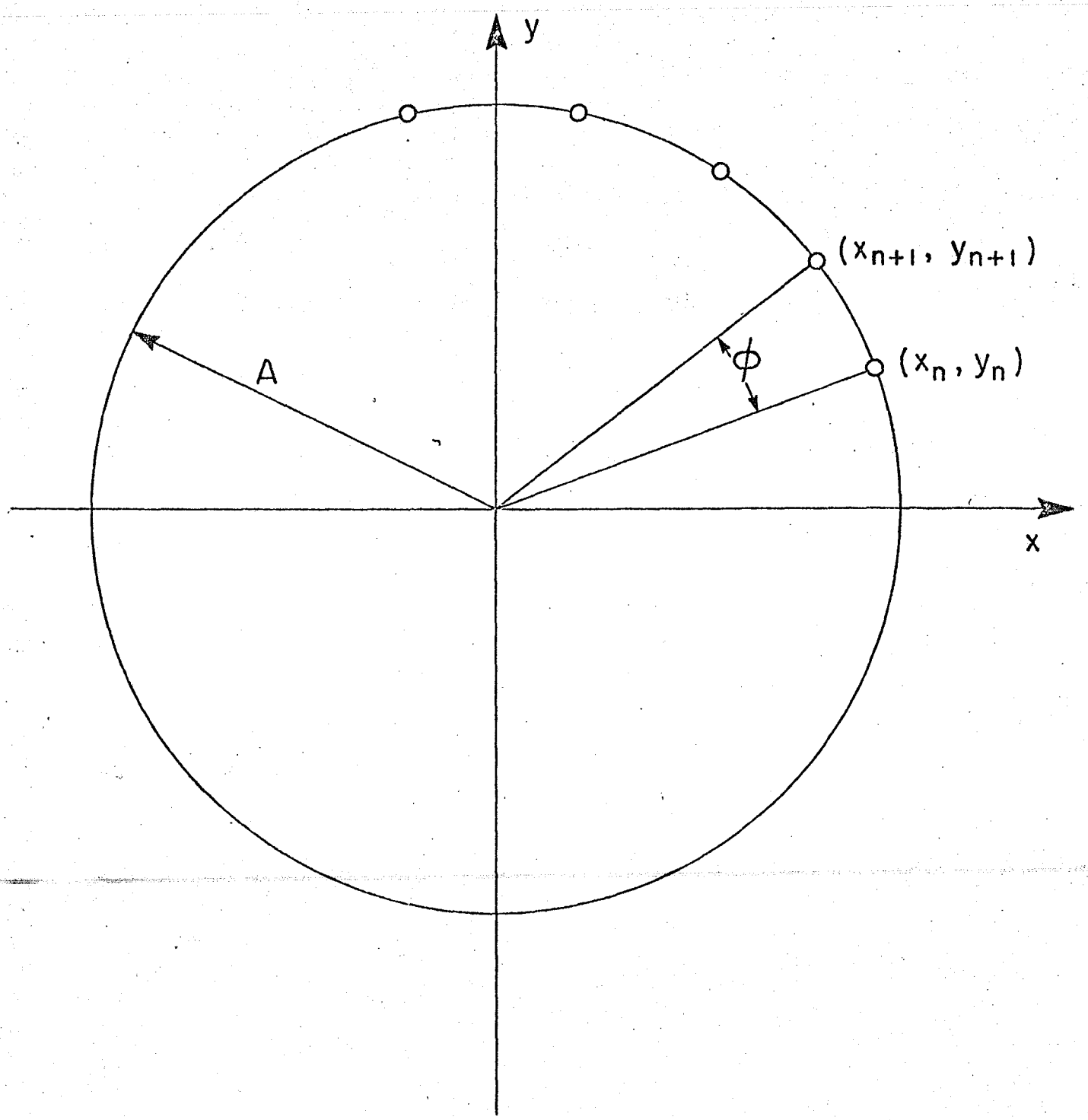

Figure 3